

Quantification of Binary Diffusion in Protein Crystals

Aleksandar Cvetkovic,[†] Cristian Picioreanu,[†] Adrie J. J. Straathof,^{*,†} Rajamani Krishna,[‡] and Luuk A. M. van der Wielen[†]

Department of Biotechnology, Delft University of Technology, Julianalaan 67, 2628 BC Delft, The Netherlands, and Van 't Hoff Institute for Molecular Sciences, University of Amsterdam, Nieuwe Achtergracht 166, 1018 WV Amsterdam, The Netherlands

Received: January 17, 2005; In Final Form: April 1, 2005

The use of confocal laser scanning microscopy for visualization and quantification of binary diffusion within anisotropic porous material is described here for the first time. The dynamics of adsorption profiles of dianionic fluorescein, zwitterionic rhodamine B, and their mixture in the cationic native orthorhombic lysozyme crystal were subsequently analyzed. All data could be described by a classical pore diffusion model. There was no change in the adsorption characteristics, but diffusion decreased with the introduction of a second solute in the solution. It was found that diffusion is determined by the combination of steric and electrostatic interactions, while adsorption is dependent on electrostatic and hydrophobic interactions. Thus, it was established that the outcome of binary transport depends on the solute, protein, and crystal characteristics.

Introduction

A rapid surge in the number of resolved protein crystal structures has occurred because of enhanced ability for the determination of optimal crystallization conditions by atomized screening techniques,¹ theoretical predictions on the basis of the second virial coefficient,² or protein engineering¹ and easier characterization of protein crystallization.¹ Protein nanocrystals have been produced and characterized,³ large scale crystallization processes for the production of uniform protein crystals with sharp cutoff crystal sizes have been described and developed,⁴ and crystals made of monoclonal antibodies have successfully been applied in enantioselective separations.⁵ These noteworthy advances provide support for the applications of protein crystals, in separation processes such as chromatography,^{6–8} in enzymatic production processes,^{9–13} in medical formulations for pharmaceutical delivery,^{14–16} in biosensors,^{17,18} and in detergents.⁹

The combination of the crystals' open structure (a high porosity and pore surface area) with the wide variety of molecular topologies and with the proteins' ability of regio- and stereoselective recognition makes protein crystals a novel class of nanoporous materials⁶ of vital interest for many industrial fields. Despite the progress made in improving the characteristics of protein crystals, comprehension of solute transport phenomena in the crystal pores is still modest. In the case of single-solute uptake, significant progress has been achieved. Solute diffusion in protein crystals was found to be anisotropic^{19,20} and dependent on steric interactions in the pores.²⁰ Electrostatic and hydrophobic characteristics of both the solute and the crystals dictated solute adsorption by protein crystals.^{21,22} Real processes, involving multicomponent transport and adsorption, have not been investigated; therefore, they may or may not be realistically represented by a combination of single-solute data. The true challenge in dealing with actual

processes is a quantitative comprehension of multicomponent phenomena, which will be the subject of this paper.

Confocal laser scanning microscopy (CLSM), being the only available experimental technique capable of simultaneous spatial and temporal monitoring in situ, has already been applied to study single-solute diffusion in isotropic^{23–29} and anisotropic materials.¹⁹ Furthermore, the same technique has been used for visualization of the binary uptake of labeled proteins by isotropic spherical materials. However, there are no measurements of such processes in anisotropic materials. Therefore, the methods for qualitative¹⁹ and quantitative²⁰ studies of fluorescein diffusion in native lysozyme crystals of different structures will be adopted in this paper to enable the quantitative visualization of the in situ binary diffusion in anisotropic porous material.

Quantitative analysis of the binary diffusion of fluorescein and rhodamine B in native orthorhombic lysozyme crystals was performed. Orthorhombic lysozyme, being the most anisotropic of all lysozyme structures, is chosen as the model crystal. The properties of lysozyme and the morphologies of its crystals are well-known, and the crystals can be obtained easily and reproducibly. Fluorescein and rhodamine B are suitable solutes for this study because of their fluorescence, their similarity in structure, and their difference in charge.

Materials and Methods

Materials. Chicken egg-white lysozyme was obtained from Sigma (Product No. L-6876; 95% purity; $M = 14\,307\text{ g mol}^{-1}$) and was used without further purification. Orthorhombic structures of lysozyme crystals were prepared according to the procedure described by Cvetkovic et al.¹⁹ The disodium salt of fluorescein (Sigma, Product No. F-6377) and the hydrochloride of rhodamine B (Fluka, Product No. 83690) were used without further purification.

Preparation of the Solutions. The mother liquor of crystallization was filtered using Schleicher & Schuell (Germany) syringe filters with a cutoff value of 200 nm, and a concentrated solution of sodium fluorescein or/and rhodamine B was added until the desired concentration was reached. Solutions of

* Author to whom correspondence should be addressed. Phone: +31-15-2782330. Fax: +31-15-2782355. E-mail: a.j.j.straathof@tnw.tudelft.nl.

[†] Delft University of Technology.

[‡] University of Amsterdam.

TABLE 1: Distribution Coefficient K of Rhodamine B and Fluorescein between the Mother Liquor Solution and the Native Orthorhombic Crystals

x_{fl}^0	pH ⁰	pH ^{eq}	distribution coefficient (K)	
			fluorescein	rhodamine B
1.000	8.36	8.79–8.92	14.66 ± 0.078	
0.735	8.53	8.70–8.89	12.78 ± 0.069	67.27 ± 0.538
0.495	8.54	8.58–8.85	13.74 ± 0.120	60.35 ± 0.561
0.2573	8.53	8.67–8.91	18.05 ± 0.157	56.78 ± 0.505
0.000	8.66	8.70–8.85		55.03 ± 0.315

^a x_{fl}^0 is the fluorescein fraction of total solute concentration in the initial solution ($x_{\text{fl}}^0 = 1 - x_{\text{rh}}^0$).

TABLE 2: Constants (k) for the Determination of the Individual Solute Concentrations in Their Mixtures

	batch experiments		CLSM experiments	
	$\lambda = 490$ nm	$\lambda = 556$ nm	$\lambda = 505$ –530 nm	$\lambda = 560$ –615 nm
fluorescein	1	0.0874	1	1
rhodamine B	0.001	1	0.001	0.084

fluorescein, rhodamine B, and their mixtures (1:1) with an initial cumulative concentration of 4.39 $\mu\text{mol L}^{-1}$ were used in CLSM diffusion experiments, whereas three solutions of fluorescein (4.39, 13.27, and 33.36 $\mu\text{mol L}^{-1}$), two solutions of rhodamine B (4.39 and 21.11 $\mu\text{mol L}^{-1}$), and three solutions of their mixtures with cumulative concentrations of 21.34 $\mu\text{mol L}^{-1}$ (composition and pH according to Table 1) were used to investigate their adsorption characteristics. The pH of every solution was adjusted by adding 1 mol L^{-1} NaOH or HCl.

Adsorption Experiments. Finite batch experiments were performed according to a procedure described elsewhere.²² For single-component systems, dye concentrations in the supernatant solution were determined by measuring solution absorbance (E) using a UV–vis spectrophotometer (Pharmacia, Ultrospec III) at the wavelengths of their maxima, 488 and 556 nm for fluorescein (λ_1) and rhodamine B (λ_2), respectively. Fluorescein and rhodamine B adsorption spectra overlap at a wavelength of 488 nm, so fluorescein concentrations in the equilibrated binary solution could not be directly determined. The procedure of Porter³⁰ was slightly modified to obtain the correct concentration of the components in a binary solution from the measured solution absorbencies at 488 and 556 nm (E_{λ_1} and E_{λ_2}) using the following equations

$$C_{\text{fl}}^{\text{L}} = \frac{k_{\text{fl},1}E_{\lambda_1} - k_{\text{fl},2}E_{\lambda_2}}{k_{\text{fl},1}k_{\text{rh},2} - k_{\text{fl},2}k_{\text{rh},1}} \quad (1)$$

$$C_{\text{rh}}^{\text{L}} = \frac{k_{\text{rh},2}E_{\lambda_2} - k_{\text{rh},1}E_{\lambda_1}}{k_{\text{fl},1}k_{\text{rh},2} - k_{\text{fl},2}k_{\text{rh},1}} \quad (2)$$

The parameters ($k_{\text{fl},1}$, $k_{\text{fl},2}$, $k_{\text{rh},1}$, and $k_{\text{rh},2}$) represent the ratio between the absorbance of a solute (fluorescein and rhodamine B) and the absorbance of the solute with an absorbance maximum at the measured wavelength of 488 nm (λ_1) or 556 nm (λ_2). Parameter values are shown in Table 2. The solute concentrations in the crystals were calculated from their solution concentrations by establishing mass balances for solute over the system with the assumption of zero initial concentration of the solutes in the crystals.

The data obtained from finite batch adsorption experiments were used to estimate linear distribution coefficients (K) of the solutes in the system

$$\frac{q_j^{\text{eq}}}{C_j^{\text{L,eq}}} = \rho^{\text{cr}} K_j = Q_{\text{sat},j} b_j \quad (3)$$

where q_j^{eq} and $C_j^{\text{L,eq}}$ are the crystal and liquid concentrations of component j at equilibrium, b_j and Q_{sat} are the adsorption affinity and capacity, respectively, in the Langmuir isotherm, and ρ^{cr} is the density of the crystal.

Confocal Laser Scanning Microscopy. A SP2-AOBS confocal system from Leica (Mannheim, Germany) mounted on a RX-A Leica microscope (Wetzla, Germany) in the fluorescence mode was employed to produce confocal images of the diffusion process. The system was equipped with two lasers, a green helium–neon and an argon ion, each with an acousto-optic tuneable filter in front permitting the precise selection of excitation intensity. Fluorescein was excited at a wavelength of 488 nm and rhodamine B at 543 nm. Two photomultipliers of the confocal system allowed simultaneous detection of two signals at different spectral ranges. Thus, emitted fluorescent light was detected at 505–530 nm and 560–615 nm for fluorescein and rhodamine B, respectively. Confocal images were obtained with an N-PLAN 20.0 \times 0.50 numerical aperture objective lens. The experimental setup and procedure have been described in detail elsewhere.^{19,20}

Individual orthorhombic crystals were analyzed by obtaining confocal images of the optical xy plane (perpendicular to the laser beam) during the scanning of the crystal starting from a horizontal plane at the base of the crystal and at constant vertical intervals up to the upper surface of the crystal. For background and noise reduction, the images were generated by accumulating four scans per image, and suitable laser illumination was chosen to avoid photobleaching. The image size was 512 \times 512 pixels.

Typically, 25 to 40 images at different diffusion times were taken per experiment. The first scan was after maximally 15 min. Initially, intervals between images were 10 min. After 2 h, intervals were increased to 20 min, and after 4 h they were increased to 1–2 h. Scanning was stopped after 24–36 h, depending on the size of the crystal. Diffusivities were calculated with 3–5 images generated at different diffusion times per crystal used. Finally, the diffusivities shown in Table 3 were obtained by averaging the results of duplicate or triplicate experiments performed with different crystals.

To correct for the overlap of fluorescein and rhodamine B fluorescence emission, the correction procedure described by eqs 1 and 2 was applied using $\lambda_1 = 505$ –530 nm (fluorescein) and $\lambda_2 = 560$ –615 nm (rhodamine B). The parameter values utilized in the correction procedure are shown in Table 2 and were determined from the data for the saturated crystal.

Modeling the Anisotropic Diffusion. Diffusion Equation. Since an anisotropic diffusion model was found to be appropriate to describe single-solute diffusion in the protein crystals,²⁰ it was applied also in this study. The time-dependent intraparticle continuity equation for the anisotropic pore diffusion model is described by²⁰

$$\frac{\partial C_p}{\partial t} = D_{xx} \frac{\partial^2 C_p}{\partial x^2} + D_{yy} \frac{\partial^2 C_p}{\partial y^2} + D_{zz} \frac{\partial^2 C_p}{\partial z^2} \quad (4)$$

where D_{ii} are elements of the effective pore diffusion matrix (D_p) representing the pore diffusivities in the orthogonal crystal directions ($i = x, y, \text{ or } z$) and C_p is the solute concentration in the crystal pores. Diffusion in the crystal can be described without including cross diffusivities.²⁰

TABLE 3: Diffusion Coefficients of Solutes in Diagonal Directions of Orthorhombic Lysozyme Crystals Determined from the Single and the Binary Diffusion Experiments together with the Hydrophobicity and Charge of the Corresponding Crystal Pores and Sizes of the Solutes

name	solute parameters			crystal direction	unit cell direction	crystal parameters			diffusivity/ 10^{-15} $\text{m}^2 \text{s}^{-1}$	
	equivalent diameter d_s/nm	hydrophobicity ^c $\log K_{\text{oct-wat}}$	charge			equivalent diameter ^a d_p/nm	density of hydrophobicity in pores/ nm^{-3}	charge density in pores/ nm^{-3}	single	binary
fluorescein	0.69 ± 0.02^a	4.05	dianion	x	a	0.74 ± 0.04	0.32	0.023	7.1 ± 1.2	3.0 ± 0.4
				z	b	1.01 ± 0.05	0.97	-0.039	210 ± 20	135 ± 11
				y	c	1.97 ± 0.06	0.76	0.158	700 ± 45	534 ± 42
rhodamine B	0.75 ± 0.03^b	5.54	zwitterion	x	a	0.74 ± 0.04	0.32	0.023	4.1 ± 0.6	1.8 ± 0.4
				z	b	1.01 ± 0.05	0.97	-0.039	200 ± 30	185 ± 17
				y	c	1.97 ± 0.06	0.76	0.158	410 ± 25	330 ± 27

^a From Cvetkovic et al.¹⁹ ^b Calculated using procedure described Cvetkovic et al.¹⁹ ^c From Cvetkovic et al.²¹

To describe single-component diffusion in anisotropic pore material, three parameters (i.e., diffusivities D_{ii}) are required; therefore, six parameters are needed for the description of two-component diffusion. This might lead to unstable computations and raise issues of reliability and sensitivity of the parameters obtained by numerical optimization procedures. As an alternative to this procedure, we employed a simplified approach in which the diffusion of every component in the two-component system is treated as if it represents a single-component diffusion. Thus, two-component diffusion can be described by eq 4 wherein the diffusion coefficients represent single-solute diffusivity corrected for the presence of the second diffusing solute.

Boundary and Initial Conditions. Computations were performed in a rectangular domain large enough to contain the modeled crystal. The initial values (at $t = 0$) of C_p were set to zero in the interior of the crystal and were set to C_p in the sub-domain outside the crystal. As a boundary condition for eq 4, the concentration outside the crystal was kept constant at any time, which is a good approximation in the experimental conditions studied. Considering the sensitivity of the diffusion model on the position of the crystal boundaries, a criterion was added that defines the boundary as the set of points with the highest intensity on a line from the crystal center to the crystal surface.²⁰

Numerical Methods. Equation 4 was discretized with finite differences in three-dimensional (3-D) space on a grid of size (Δx , Δy , Δz). A forward explicit discretization in time was found to give sufficient accuracy at time steps between 0.1 and 1 s and was preferred for simplicity.³¹ After computing concentration fields at different diffusion times, a Simplex optimization algorithm³¹ was used to fit the model calculations to the experimental data by varying the diffusion coefficients. A least-squares criterion was applied for minimizing the difference between measured profiles and calculated profiles. The fitting procedure was applied separately for data obtained at three different diffusion times. The computer program was written by our group in C++ and run on a desktop PC.²⁰

Determination of the Pore Charges and Hydrophobicity. Each functional group in a protein molecule was assumed to contribute in an additive manner to the value of $\log K_{\text{oct-wat}}$. $K_{\text{oct-wat}}$ is the octanol–water distribution constant, which represents the hydrophobic character of the molecule.³² These contributions are accurately known for the side chain of each residue in amino acid structures.^{33,34} In the same manner, $\text{p}K_a$ values of the side chains of all amino acid residues were taken from the literature.³⁵ The commercial software package PyMOL³⁶ was utilized for the determination of each pore’s hydrophobicity and charge at a given pH. The positions of the atoms in a crystal structure were imported from the Protein Data Bank (PDB code 1AKI) into PyMOL, which was used to produce protein structures consisting of several unit cells in all

three crystallographic directions. Van der Waals representations of the atomic radii were used. For every amino acid residue, its location in the crystal was determined using the following assumptions:

(a) Considering that the size of a pore in the direction of a diffusion front determines solute diffusivity,²⁰ only the pore space in that direction was taken into account. Therefore, imaginary borders were imposed on each pore crossing.

(b) The amino acid residues of the protein in touch with the pore were counted.

(c) The amino acid residues can belong only to one pore. Residues in the pore crossings belong to the pore to which they contribute the most (in terms of pore wall surface).

Three separate files were made representing one pore section (one pore with a length of three unit cells) for each orthogonal crystal direction. The charge density of the pores (d_{el}) was determined using the following equation

$$d_{\text{el}} = \frac{n_p \sum m_i Z_i}{V_{\text{uc}}} \quad (5)$$

where n_p is number of pores in the unit cell, m the number of amino acid residues i in one pore, Z the charge of amino acid residue i , and V_{uc} the volume of the crystal unit cell. The hydrophobic density of the pores was also calculated by eq 5, where instead of Z a $\log K_{\text{oct-wat}}$ value was used.

Results and Discussion

Determination of the Diffusion Coefficients. Diffusion into porous materials is determined by the intraparticle diffusion and the external liquid–film mass transfer resistance. Intraparticle diffusion is the rate-limiting step in fluorescein uptake.¹⁹ This was also observed for rhodamine B uptake (data not shown).

The pore diffusion model (eq 4) can only be utilized to describe diffusion that occurs in the linear part of the adsorption isotherm. Therefore, adsorption of fluorescein and rhodamine B by native orthorhombic lysozyme crystals from solutions of different initial solute compositions was studied. Adsorption equilibrium data of fluorescein and rhodamine B for single-solute and binary systems can be fit well to eq 3 describing the linear part of the Langmuir adsorption isotherm (Figure 1). Along with the experimental conditions, the distribution coefficients (K) for fluorescein and rhodamine obtained by linear least-squares regression are summarized in Table 1. For single-solute solutions, values of K were determined for the entire range of experimentally used initial concentrations, and they were found to be independent from the initial concentration. Although there is some mutual influence of the solutes on each other’s equilibrium uptake, this influence is neglected subsequently

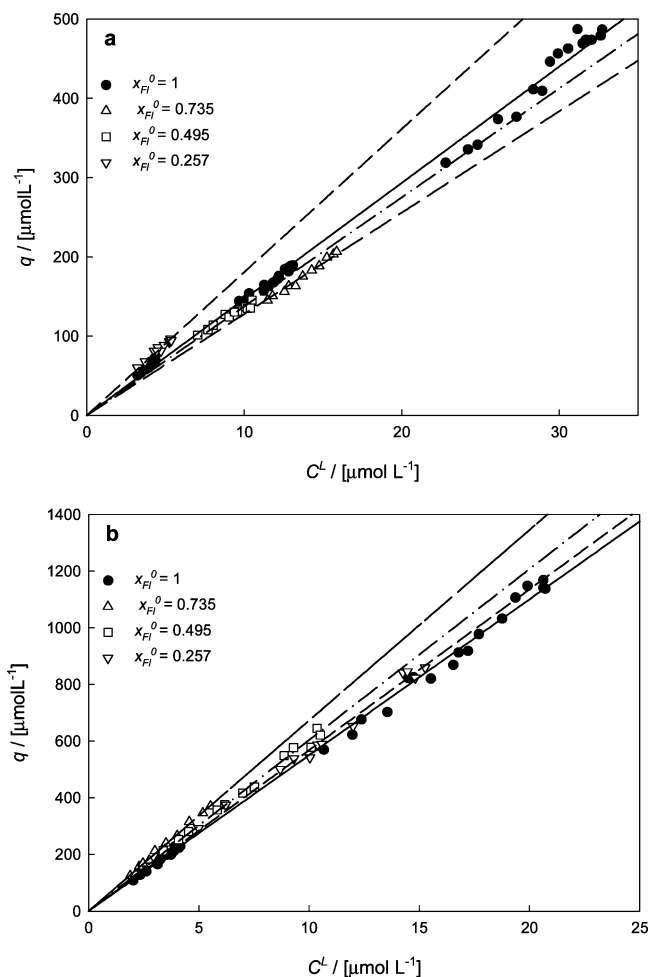


Figure 1. Adsorption of (a) fluorescein and (b) rhodamine B from single-solute and binary solutions (where x_{FI}^0 is the fluorescein fraction of the total solute concentration in the initial solution, $x_{\text{FI}}^0 = 1 - x_{\text{RH}}^0$). The markers are experimental points, and the lines are fits of eq 3.

because other mutual influences will turn out to be much larger. Furthermore, no detectable alterations in the crystals' volumes or shapes were detected, and therefore the anisotropic pore diffusion model might be suitable to depict single-solute and binary diffusion.

Obtaining and processing diffusion data by CLSM for single-solute experiments has been described in the case of fluorescein diffusion in lysozyme crystals.^{19,20} However, no attempts have been made to quantify binary diffusion in protein crystals or any other porous material. Due to the use of appropriate dichroic beam splitters and band-pass filters in front of the detector, the confocal microscope is able to detect two different fluorescence emissions simultaneously. As a result, two distinct images were obtained for fluorescein and for rhodamine B from the same particle (Figure 2). A Cartesian coordinate system was adopted for every CLSM image with the x -coordinate parallel to the short side of the crystal, the y -coordinate perpendicular to x along the long side, and the z -coordinate perpendicular to the CLSM image, representing the crystal thickness. Through the use of crystallographic knowledge, the coordinate system used in our study (x, y, z) was connected to the unit cell coordinate system (a, b, c) as shown in Table 3.

A typical example for comparison of experimental data collected by CLSM and calculated solute concentration profiles for binary diffusion is presented for fluorescein in Figure 3 and rhodamine B in Figure 4. Solute concentration profiles in the

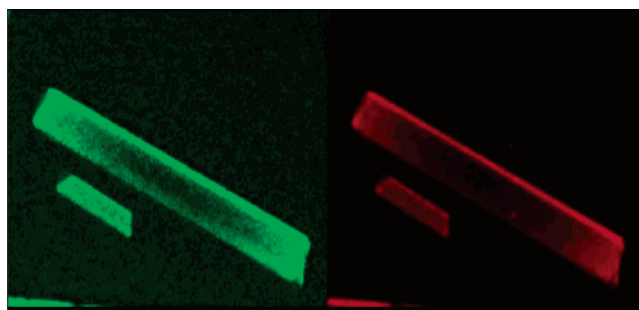


Figure 2. Confocal images of the simultaneous diffusion of fluorescein (left) and rhodamine B (right) into native orthorhombic lysozyme crystals.

crystals can be well-represented by the anisotropic pore diffusion model at the positions shown in Figures 3 and 4 or at any other (x, y, z) position in the crystals (data not shown). Differences between the model predictions and experimental data (the error images in Figures 3 and 4) are attributed to simplifying assumptions of the diffusion model (homogeneous materials with smooth outer surfaces) whereas the actual crystal is characterized by the presence of defects, surface roughness, charge and pore distributions, and heterogeneity of the refractive index. Such observations were also made for the two types of single-solute diffusion in the orthorhombic structure.

Comparison of Single-Solute Diffusion Coefficients. To understand the behavior of the solute mixture, comprehension of the behavior of the individual solutes in single-solute systems is required. Fluorescein single-solute diffusion in the crystal pores of three different crystal structures was dependent on the solute to pore size ratio.²⁰ Size exclusion was established as a main mechanism.²⁰ The single-solute diffusion of rhodamine B in the native orthorhombic crystal follows the same trend (Table 3).

Note that in Table 3 the equivalent diameter calculated for rhodamine B (d_s) is slightly larger than that calculated for the pores in the a crystal direction (d_p). Still, rhodamine B enters the crystal through these pores. This is due to the simplifications in these calculations. Considering that neither the crystal pores are cylindrical nor the solute ions are spherical, equivalent diameters only represent the smallest projection area of the pore and the mean projection of area of solute ions. Using space-filling models, we determined that rhodamine can be fit in the crystal pores.

However, several more serious deviations from the size exclusion model were detected (Figure 5). At $d_s/d_p \approx 0.35$, the two solutes showed widely different diffusivities. In view of the size scale of the crystal pores and solutes (the distance between the solutes and the pore walls is below 0.6 nm), both electrostatic and hydrophobic interactions can contribute to diffusion in protein crystals. The hydrophobicity and charge characteristics of the solutes and pores were calculated and are summarized in Table 3. An influence of the electrostatic interactions is clear from the data in Table 3. In the negatively charged b pores, both solutes diffuse at almost the same rate despite their about 10% size difference. In the positively charged a and c pores, diffusion of negatively charged fluorescein is much faster than expected on the basis of the 10% size difference with zwitterionic rhodamine B.

Diffusion is generally faster for the dianionic fluorescein than for zwitterionic rhodamine B (Table 3), and adsorption is stronger for rhodamine B (Table 1), which is contrary to the expectations from simulations of diffusion in protein crystals,³⁷ wherein for oppositely charged solute-sorbent systems adsorp-

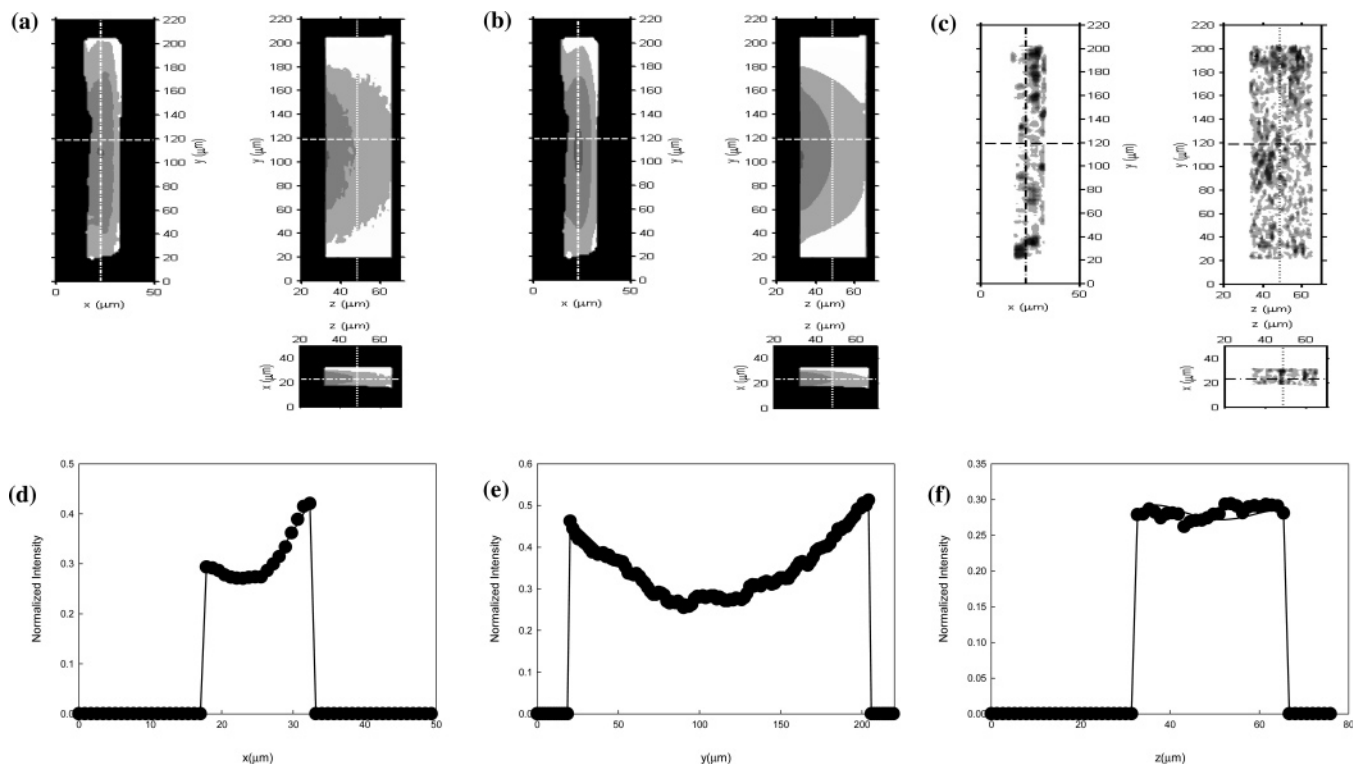


Figure 3. (a) Planar cross sections of fluorescence intensity data experimentally obtained by CLSM after 2100 s of fluorescein diffusion in an orthorhombic lysozyme crystal from a binary mixture. (b) Model-computed solute concentrations at 2100 s, shown in a gray scale with darker areas corresponding to lower concentrations. (c) Spatial distribution of the deviation between experimental and computed data (error maps), for the distributions presented in plots a and b. In the gray scale, the black areas represent the points with the highest discrepancies, and white represents a perfect correspondence; (d–f) Cross sections through the lysozyme crystal showing the experimental points (markers) and calculated profiles using the 3-D diffusion model (lines). The cross sections are along planes at $x = 23 \mu\text{m}$, $y = 119.1 \mu\text{m}$, and $z = 48.4 \mu\text{m}$, shown in parts a–c as white dotted lines.

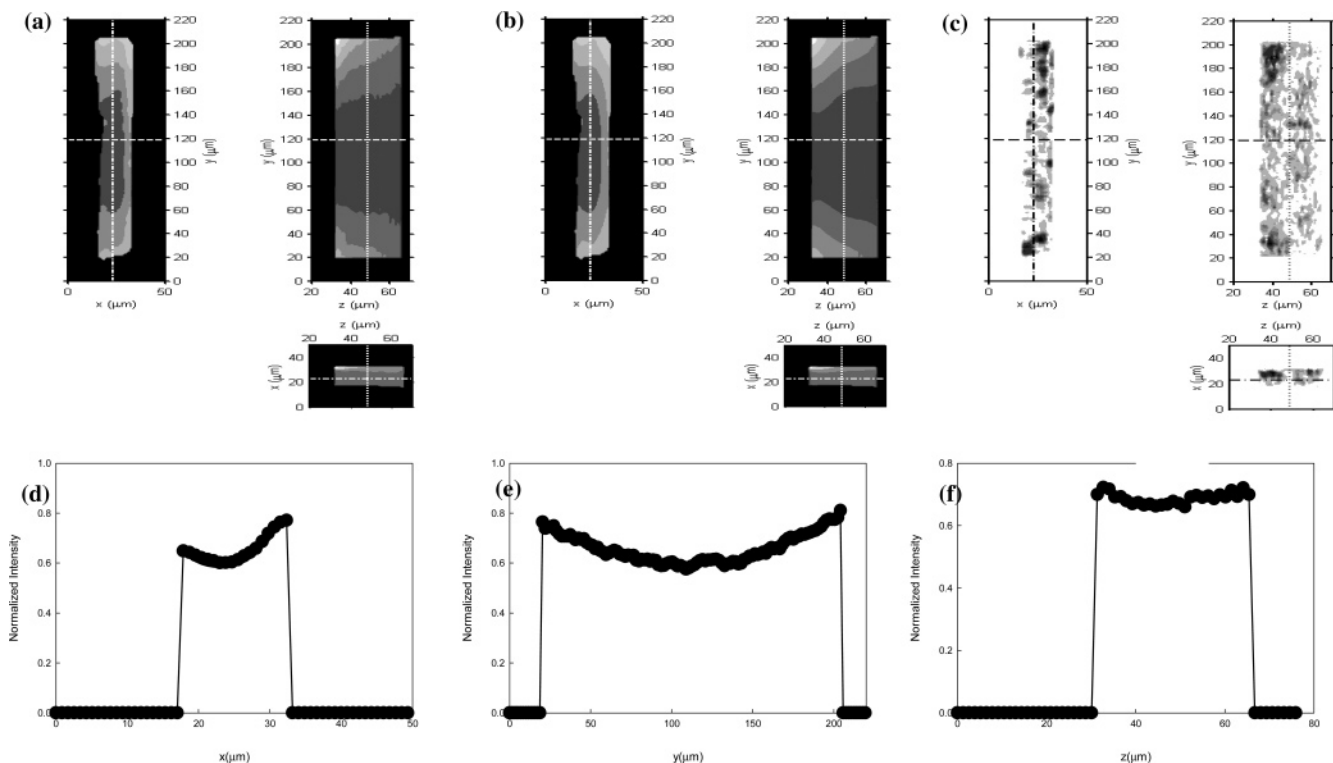


Figure 4. Rhodamine B diffusion in the orthorhombic lysozyme crystal from a binary mixture obtained at same time and the same position as for fluorescein in Figure 3.

tion is expected to be higher and diffusion to be lower. Solute adsorption in protein crystals is determined by ion exchange with a co-ion that was originally in the crystal and by

competition with co-ions in the solution.²² The presence of chloride and acetate anions, especially at high concentrations, particularly deprives fluorescein adsorption by lysozyme crys-

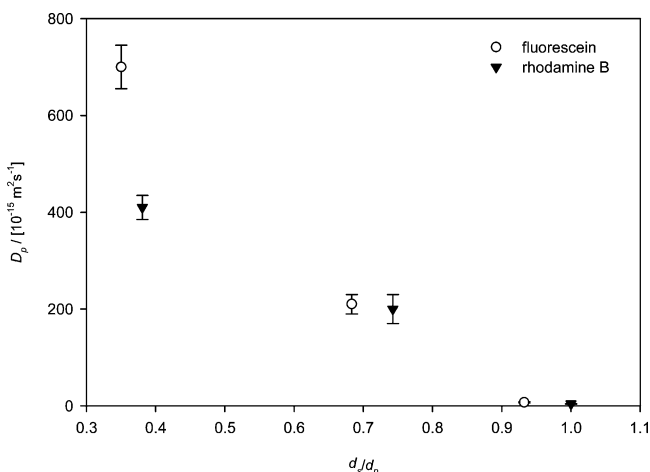


Figure 5. Pore diffusivity (D_p) of fluorescein and rhodamine B in different crystal directions determined in the single-solute experiments as a function of solute to pore size ratio.

tails,²² resulting in relatively small values for K . The influence of sodium present in the solution on the adsorption of rhodamine B by lysozyme crystals is unknown.

Therefore, the combination of a higher selectivity of lysozyme for rhodamine B than for sodium ions and a higher hydrophobicity of rhodamine B (than for fluorescein) may cause the 4 times higher adsorption and eventually the slower diffusion of rhodamine B as compared to fluorescein, despite the charges.

Binary Diffusion and Adsorption. The mechanism behind the uptake of the rhodamine B and fluorescein from their single-solute and binary solutions is the same and can be successfully described by the anisotropic pore diffusion model. Diffusion coefficients in the binary experiments are smaller than in the corresponding single-solute experiments (Table 3). Furthermore, the bigger the pore, the lower this decrease in the diffusivity. This suggests that the solutes are mutually blocking each other's diffusion by steric hindrance. Blocking of fluorescein by rhodamine B seems to be more serious than the other way around. This can be caused by the strong rhodamine B adsorption (Table 1).

Conclusions

CLSM was used for the first time for quantification of binary diffusion in anisotropic material. For the investigated systems consisting of fluorescein and rhodamine B as solutes and orthorhombic lysozyme crystal as a model crystal structure, diffusion of both solutes could be described by an anisotropic pore diffusion mechanism occurring under conditions of a favorable adsorption isotherm. Besides steric interactions, electrostatic interactions between the sorbent and the solutes determine the diffusion in protein crystals. The results indicate that the governing mechanism behind the transport of small molecules in ion exchangeable protein crystal pores depends on solute composition, solute and protein properties, and especially on the crystal intraparticle pore and charge distributions.

An understanding of transport parameters might lead to considerable improvements of present technologies and to the development of new strategies for crystal application in separation and biocatalytic processes. These improvements could be achieved either through optimization of the operation conditions or through the tailored design of crystals for a specific application using crystal and protein engineering.

Acknowledgment. The Netherlands Organization for Scientific Research—Chemical Sciences (NWO-CW) has funded

this work. It has been performed within the International Research Training Group "Diffusion in Porous Materials", jointly supported by the NWO (Netherlands) and the DFG (Germany). We are thankful to Dr. Yuval Garini from the TU Delft, The Netherlands, for providing experimental facilities and support. We thank Dr. E. S. J. Rudolph from the University of Leiden, The Netherlands, for fruitful discussions and a critical review of the manuscript.

References and Notes

- (1) McPherson, A. *J. Struct. Funct. Genomics* **2004**, *5*, 3–12.
- (2) Tessier, P. M.; Lenhoff, A. M. *Curr. Opin. Biotechnol.* **2003**, *14*, 512–516.
- (3) Martin, R. W.; Zilm, K. W. *J. Magn. Reson.* **2003**, *165*, 162–174.
- (4) Vuolanto, A.; Uotila, S.; Leisola, M.; Visuri, K. *J. Cryst. Growth* **2003**, *257*, 403–411.
- (5) Vuolanto, A.; Kiviharju, K.; Nevanen, T. K.; Leisola, M.; Jokela, J. *Cryst. Growth Des.* **2003**, *3*, 777–782.
- (6) Vilenchik, L. Z.; Griffith, J. P.; St Clair, N.; Navia, M. A.; Margolin, A. L. *J. Am. Chem. Soc.* **1998**, *120*, 4290–4294.
- (7) Margolin, A. L. *Chimia* **1996**, *50*, 423–424.
- (8) Pastinen, O.; Jokela, J.; Eerikainen, T.; Schwabe, T.; Leisola, M. *Enzyme Microb. Technol.* **2000**, *26*, 550–558.
- (9) Margolin, A. L.; Navia, M. A. *Angew. Chem., Int. Ed.* **2001**, *40*, 2205–2222.
- (10) St. Clair, N. L.; Navia, M. A. *J. Am. Chem. Soc.* **1992**, *114*, 7314–7316.
- (11) Persichetti, R. A.; Lalonde, J. J.; Govardhan, C. P.; Khalaf, N. K.; Margolin, A. L. *Tetrahedron Lett.* **1996**, *37*, 6507–6510.
- (12) Lalonde, J. J.; Govardhan, C. P.; Martinez, A. G.; Visuri, K.; Margolin, A. L. *J. Am. Chem. Soc.* **1995**, *117*, 6845–6852.
- (13) Vaghjiani, J. D.; Lee, T. S.; Lye, G. J.; Turner, M. K. *Biocatal. Biotransform.* **2000**, *18*, 151–175.
- (14) Jen, A.; Merkle, H. P. *Pharm. Res.* **2002**, *18*, 1483–1488.
- (15) Basu, S. K.; Govardhan, C. P.; Jung, C. W.; Margolin, A. L. *Expert Opin. Biol. Ther.* **2004**, *4*, 301–317.
- (16) St. Clair, N. L.; Shenoy, B.; Jacob, L. D.; Margolin, A. L. *Proc. Natl. Acad. Sci. U.S.A.* **1999**, *96*, 9469–9474.
- (17) Morozov, V. N.; Morozova, T. Y. *Anal. Biochem.* **1992**, *201*, 68–79.
- (18) de Mattos, I. L.; Lukachova, L. V.; Gorton, L.; Laurell, T.; Karyakin, A. A. *Talanta* **2001**, *54*, 963–974.
- (19) Cvetkovic, A.; Straathof, A. J. J.; Hanlon, D. N.; van der Zwaag, S.; Krishna, R.; van der Wielen, L. A. M. *Biotechnol. Bioeng.* **2004**, *86*, 389–398.
- (20) Cvetkovic, A.; Picioreanu, C.; Straathof, A. J. J.; Krishna, R.; van der Wielen, L. A. M. *J. Am. Chem. Soc.* **2004**, *127*, 875–879.
- (21) Cvetkovic, A.; Straathof, A. J. J.; Krishna, R.; van der Wielen, L. A. M. *Langmuir* **2004**, *21*, 1475–1480.
- (22) Cvetkovic, A.; Zomerdijk, M.; Straathof, A. J. J.; Krishna, R.; van der Wielen, L. A. M. *Biotechnol. Bioeng.* **2004**, *87*, 658–668.
- (23) Ljunglof, A.; Thommes, J. *J. Chromatogr., A* **1998**, *813*, 387–395.
- (24) Ljunglof, A.; Larsson, M.; Knuutila, K. G.; Lindgren, J. *J. Chromatogr., A* **2000**, *893*, 235–244.
- (25) Lowry, M.; He, Y.; Geng, L. *Anal. Chem.* **2002**, *74*, 1811–1818.
- (26) Kim, H. B.; Hayashi, M.; Nakatani, K.; Kitamura, N.; Sasaki, K.; Hotta, J. I.; Masuhara, H. *Anal. Chem.* **1996**, *68*, 409–414.
- (27) Malmsten, M.; Xing, K. Z.; Ljunglof, A. *J. Colloid Interface Sci.* **1999**, *220*, 436–442.
- (28) Rademann, J.; Barth, M.; Brock, R.; Egelhaaf, H. J.; Jung, G. *Chem.—Eur. J.* **2001**, *7*, 3884–3889.
- (29) Benda, A.; Benes, M.; Marecek, V.; Lhotsky, A.; Hermens, W. T.; Hof, M. *Langmuir* **2003**, *19*, 4120–4126.
- (30) Porter, J. F.; McKay, G.; Choy, K. H. *Chem. Eng. Sci.* **1999**, *54*, 5863–5885.
- (31) Press, W. H.; Flannely, B. P.; Teukolsky, S. A.; Vetterling, W. T. *Numerical Recipes in C: The Art of Scientific Computing*; Cambridge University Press: Cambridge, 1997.
- (32) Leo, A.; Hansch, C.; Elkins, D. *Chem. Rev.* **1971**, *71*, 525–616.
- (33) Bigelow, C. C.; Channon, M. Hydrophobicity of Amino Acids and Proteins. In *Handbook of Biochemistry and Molecular Biology*; Fasman, G. D., Ed.; CRC Press: Cleveland, 1975; pp 209–243.
- (34) Medina-Hernandez, M. J.; Catala-Icardo, M.; Garcia-Aalvarez-Coque, M. C. *Chromatographia* **1995**, *41*, 455–461.
- (35) Kuehner, D. E.; Engmann, J.; Fergg, F.; Wernick, M.; Blanch, H. W.; Prausnitz, J. M. *J. Phys. Chem. B* **1999**, *103*, 1368–1374.
- (36) DeLano, W. L. *The PyMOL Molecular Graphics System*; 2002; <http://www.pymol.org>.
- (37) Malek, K.; Odijk, T.; Coppens, M. O. *ChemPhysChem* **2004**, *5*, 1596–1599.